SUST J Sci Tech, Vol 33 (2) 2023, 10-15 ISSN- 2959-3522

Dynamic Dielectric Properties of Yttrium (Y) Substituted $LaCoO_3$

(Received 16 February 2023, Accepted 1 February 2024)

M. O. Faruk, S. Hossain, S. Chowdhury, Ovijit Chandrow, K. Salma Akter, A. Khan and S. Naher*

Department of Physics, Shahjalal University of Science and Technology, Sylhet, Bangladesh

* Corresponding Author: S. Naher (shumsun-phy@sust.edu)

Abstract

In the present work, samples of $La_{1-x}Y_xCoO_3$, (x = 0.0, 0.2, 0.4 and 0.6) were prepared by the standard solid state reaction technique. To confirm the crystal structure, X-ray diffraction were performed at room temperature. The Whole Powder Pattern Fitting (WPPF) or Rietveld method is used for $La_{1-x}Y_xCoO_3$ samples to determine the lattice constant as well as crystal structure. The capacitance, loss tangent, conductivity, resistance and reactance have been measured as a function of frequency in the range from 20 Hz to 10 kHz. The measurement of frequency dependent capacitance shows that the decrease in capacitance and loss tangent are observed with the increase in frequency. Also the value of capacitance increases and loss tangent decreases with increasing concentration of Yttrium (Y). Also, the Cole-Cole plot shows that the grain and grain boundary resistance decreases, as a result resistivity decreases while conductivity increases with increasing concentration of Y.

Keywords: WPPF; Grain; Grain boundary; loss tangent; Perovskite.

To use dielectric materials in the construction of any type of electronic device, one must be familiar with the dielectric parameters, i. e., capacitance, C and dielectric loss (loss tangent, tanδ), of those materials. Understanding the electrical conduction mechanism and dielectric relaxation behavior of such materials, which are still poorly understood, is therefore of great importance. Further increasing the dielectric parameters of such materials is required to increase their applicability in integrated circuits with reduced feature sizes due to the low power consumption devices.

The typical formula for perovskite compounds is ABO_3, where A and B are cations in which A is bigger, O is oxide anion. Due to their electrical, magnetic, thermal, mechanical and optical properties, perovskite materials gained a lot of attention from scientists [1-7]. Moreover, the chemical composition flexibility of these materials provides significant opportunities for controlling their structural properties by substituting a variety of transition metals into the A and B cation positions [8-11]. Perovskites are particularly promising for many applications due to these characteristics.

Random access memory of ferroelectrics, multilayer ceramic capacitors, catalytic converters, magnetic field sensors, fuel cells of solid oxide (FCSOs), membranes [12-16] etc. are a few potential uses for these materials. It must comprehend that these materials' electrical and magnetic properties favor their wide range of applications. A sophisticated method for separating the contributions of the grain and the boundary of the grain to the total conduction is impedance spectroscopy. The electric response is obtained using the impedance approach across a broad frequency range. The motions of the charge carrier in an electric field by displacement of charge, reorientation of dipole, creation of space charge, may be responsible for the contribution to the electric response [17-23]. The design of cutting-edge and highly effective electronic technology heavily relies on dielectric materials. It is frequently possible to individually extract additional helpful information about the examined dielectric materials using the dielectric, impedance, and modulus measurements. The modulus and impedance peaks precisely overlap due to the long-range fundamental conductivity [24-26]. We may learn more about these materials' numerous applications by focusing on their electrical characteristics. Among the

applications are electro-optic devices, detectors, and actuations in microelectro-mechanical systems.

Experimental

The pure and Y doped $LaCoO_3$ powders were prepared via standard solid state reaction technique. For synthesis of pure $LaCoO_3$, La_2O_3(≥99.9% pure) and Co_2O_3 (≥99.9% pure) powders were mixed as reactants. For the preparation of different concentrated Y doped $LaCoO_3$ powders, Y_2O_3(≥99.9% pure) powders were mixed with La_2O_3(≥99.9% pure) and Co_2O_3 (≥99.9% pure) powders. For each powder sample the identical synthesis steps were maintained. Stoichiometric ratios of the reactants were mixed together using an agate mortar for 5 hours in presence of ethanol and then the resulting mixture was calcined at 800°C for 5 hours in the air. The calcined powder was grinded for 5 hours after being taken out from the furnace in order to achieve homogeneity. The samples were then compressed (2500 N) to get the pellets using a hydraulic press, and sintering was performed for five hours at a temperature of 1300°C with a temperature ramp temperature 5°C/min in air. High-intensity X-ray (Cu-K_α) diffraction experiments were performed to assess the phase purity of the sintered pellets. The theoretical density ρ_{th} was calculated using the following expression, $\rho_{th} = 2M_A/(N_a a_0^3)$, where N_A is Avogadro's number, M is the molecular weight. The porosity was calculated from the relation, P(%) = {100 × (ρ_{th} - ρ_B)/ρ_{th}}, where ρ_B is the Bulk density determined by the Archimedes' principle. The dielectric characteristics (capacitance, loss tangent, tanδ) and electrical (impedance) characteristics of disk-shaped specimens were investigated at room temperature in the frequency range 20 Hz-10 kHz with the help of Wayne Kerr 6500B, a precision impedance analyzer. Measurements of the impedance spectroscopy were conducted for a frequency range of 100 Hz to 120 MHz at room temperature.

Results and Discussions

Lattice Parameters, Density, and Porosity

Figure1 illustrates the X-ray diffraction (XRD) patterns for the polycrystalline $La_{1-x}Y_xCoO_3$ (x = 0.0, 0.2, 0.4, and 0.6) samples sintered at 1300°C. The observed peak-positions matched well with the reported values [27] and this confirms that the synthesized materials crystallized successfully. The diagram also shows a further peak near 2θ = 29º associated with Co_2O_3 impurity phases. The observed diffraction spectra were presented in Table-1 through Rietveld refinement with the ICDD (International Centre for Diffraction Data) data. Table-1 expresses that the decreasing of lattice parameters appeared with increasing the doping of Y for all the compositions since the radius of the La^{3+} (1.06 Å) is greater than that of the Y^{3+} (1.01 Å).

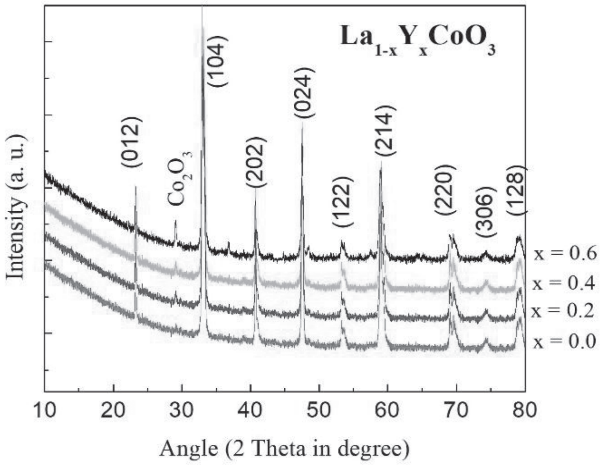

Figure 1. X-ray diffraction pattern for $La_{1-x}Y_xCoO_3$ (x = 0.0, 0.2, 0.4 and 0.6) at room temperature.

Hence, the lattice constant decreases linearly with the increase in Y content in the perovskite structure following Vegard's law. The parents $LaCoO_3$ has a rhombohedral perovskite type structure with space group $R\bar{3}c$. Upon adding the Y concentration on Polycrystalline $La_{1-x}Y_xCoO_3$, has a rhombohedral distorted perovskite type structure with space group Pnma structure from rombohedral structure with space group $R\bar{3}c$. The quality of refinement technique is examined by the goodness of the fit indicator χ^2. The refined crystallographic parameters and corresponding fit indicators for all the samples are outlined in Table-1.

Table 1. The lattice parameters, angle between them and fitting (S and R_{wp}) parameters.

Content, x	a(Å)= b(Å)	c(Å)	α(º)= β(º)	γ(º)	χ^2/S	R_{wp}
0.0	5.443	13.099	90	120	1.205	3.67
0.2	5.431	13.153	90	120	1.302	3.92
0.4	5.434	13.155	90	120	1.254	3.83
0.6	5.426	13.136	90	120	1.425	4.21

Density plays a crucial role in determining dielectric, electric as well as magnetic properties. The obtained

theoretical density, Bulk density, and porosity for the samples are listed in Table 2.

Table 2. The Theoretical density, Bulk density, Porosity of the $La_{1-x}Y_xCoO_3$ (x = 0.0, 0.2, 0.4 and 0.6) samples sintered at 1300°C temperature with a fixed dwell time of 5 hours in the air.

Content, x	Theoretical density, $\rho_{th}(gm/cm^3)$	Bulk density, $\rho_B(gm/cm^3)$	Porosity, P%
0.0	6.23	5.06	27.333
0.2	6.06	4.83	27.622
0,4	5.87	4.64	27.817
0.6	5.38	4.51	28.013

The density of all the samples decreases as the Y concentration increases for both theoretical and bulk densities. This may be due to the fact that the density of Y is 4.472 gm/cm^3 which is lower than that of La which is 6.146 gm/cm^3.

Dielectric properties

Capacitance

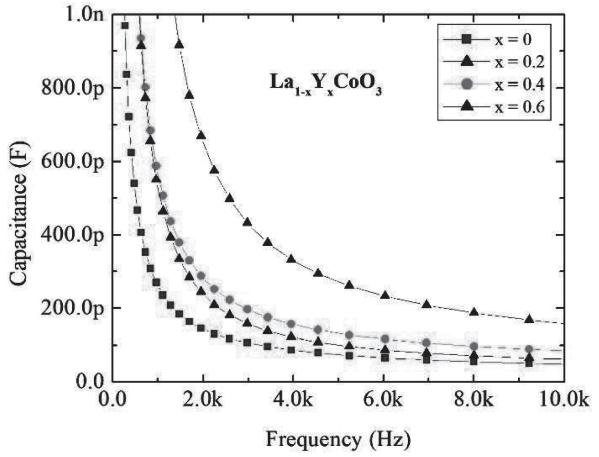

Figure 2. Frequency dependent capacitance for $La_{1-x}Y_xCoO_3$ (x = 0.0, 0.2, 0.4 and 0.6).

The capacitance of Y-doped $LaCoO_3$ measured at room temperature over frequency range 20 Hz-10 kHz is plotted in Figure 2. As can be seen, each curve of the dielectric spectra shows a drastic decrease beginning from about 1 kHz and the plateau varies negligibly for Y substitution. The loss tangent of Y-doped $LaCoO_3$ over the frequency range of 20 Hz-10 kHz is plotted. In this Figure, the capacitance of all the samples of $La_{1-x}Y_xCoO_3$ (x = 0.0, 0.2, 0.4 and 0.6) is high at low frequency and each of the capacitance curves shows a sharp decrease up to 1 kHz. After this frequency the variation is very small. From these figures it is inferred that the capacitance is increased with increasing Y doping in $LaCoO_3$ which is desired for many applications like capacitors. The frequency dependent capacitance of $La_{1-x}Y_xCoO_3$ (x = 0.0, 0.2, 0.4 and 0.6) sintered at 1300°C temperatures for five frequency values are presented in Table-3.

Table 3. The frequency dependent capacitance $La_{1-x}Y_xCoO_3$ (x = 0.0, 0.2, 0.4 and 0.6).

Frequency (kHz)	Capacitance (pF)			
	x = 0.0	x = 0.2	x = 0.4	x = 0.6
1	278	510	588	151
2	146	250	288	661
3	107	157	197	430
4	874	121	157	333
5	740	980	135	270

Loss tangent

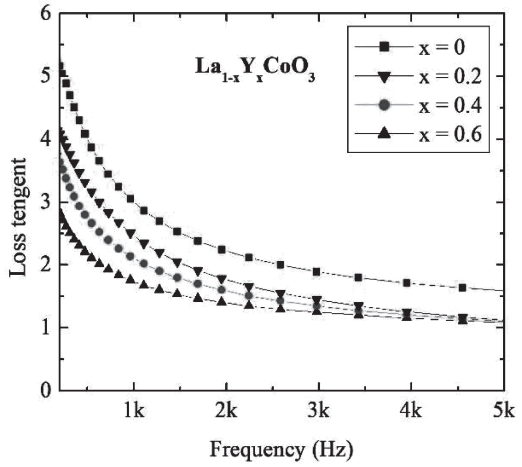

Figure 3. Frequency dependent Loss tangent for $La_{1-x}Y_xCoO_3$ (x = 0.0, 0.2, 0.4 and 0.6).

The loss tangent of Y-doped $LaCoO_3$ measured at room temperature over frequency range 10 Hz-5 kHz is plotted in Figure 3. The loss tangent of all the samples of La_{1-}

$_xY_xCoO_3$ (x = 0.0, 0.2, 0.4 and 0.6) decreases rapidly from 20 Hz to 1 kHz and remains almost the same after 1 kHz. Figure 3 illustrates that the dielectric loss decreases with increasing Y doping in $LaCoO_3$ which is desired for many applications like capacitors. The loss tangent (tanδ) of

$La_{1-x}Y_xCoO_3$ (x = 0.0, 0.2, 0.4 and 0.6) sintered at 1300°C for five frequency values are presented in Table 4.

Table 4. The loss tangent of $La_{1-x}Y_xCoO_3$ (x = 0.0, 0.2, 0.4 and 0.6) sintered at 1300°C for 5h in air.

Frequency (kHz)	Loss Tangent			
	x = 0.0	x = 0.2	x = 0.4	x = 0.6
1	3.05	2.50	2.10	1.75
2	2.21	1.78	1.60	1.40
3	1.89	1.44	1.33	1.24
4	1.70	1.25	1.21	1.20
5	1.56	1.13	1.11	1.10

Electrical properties

The lines are the fitted curves of the real and imaginary parts of the impedance (Z'-Z") obtained by plotting on the impedance complex plane at room temperature applying the Cole-Cole empirical relation. Z' vs Z" of four different compositions are plotted in Figure 4. All four curves are matched with the Cole-Cole law precisely, and the fitting parameters are shown in Table-5

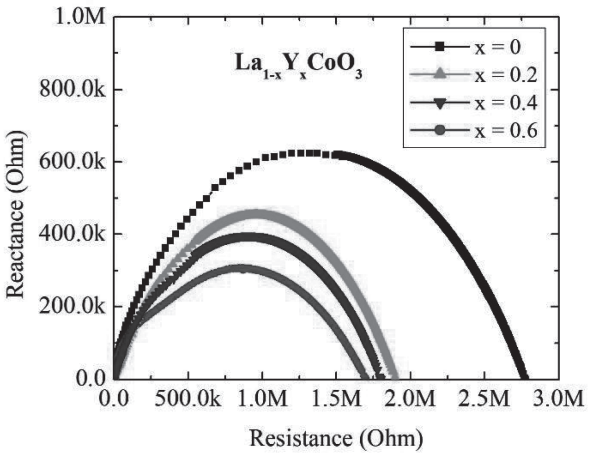

Figure 4. Cole-Cole plot with interpolation for polycrystalline $La_{1-x}Y_xCoO_3$ (x = 0.0, 0.2, 0.4 and 0.6).

An impedance spectrum analysis has been used to determine the values of the resistance of the semiconducting grain (R_{sc}) and the resistance of the insulating barriers (R_{ins}) [28] which is illustrated conceptually in Figure 4. The resistance of the semiconducting grain is found from the non-zero intercept on the Z'-axis (R_{sc}). Because of the limited frequency range at room temperature, we are aware that only a subset of the arcs can be reached by experimentation. For this reason, the well-known Cole-Cole empirical relation was used to fit and extrapolate data in order to determine the resistance of the insulating barriers (R_{ins}). It can be concluded from Sinclair's work [29] that intercepts at the low-frequency represent boundary resistance (R_{ins}). These values correlate satisfactorily to low frequency (1 kHz) loss tangent value of 3.05 for x = 0.0, 2.50 for x = 0.2, 2.10 for x = 0.4 and 1.71 for x = 0.6 of $La_{1-x}Y_xCoO_3$ (x = 0.0, 0.2, 0.4 and 0.6) compositions. This proves that the low-frequency rise in loss tangent (tanδ) can be attributed to the boundary resistance.

Table 5. Fitting parameters of Cole-Cole plot for $La_{1-x}Y_xCoO_3$ (x = 0.0, 0.2, 0.4 and 0.6) samples sintered at 1300°C temperatures with fixed dwell time 5 hours in air.

Content, x	α	R_{sc}(Ω)	R_{ins}(Ω)	Conductivity(s/m) at 10kHz
0	0.92	1647	2780663	1.15E-04
0.2	0.91	1635	1915584	1.22E-04
0.4	0.94	1618	1813852	1.83E-04
0.6	0.95	1571	1695526	2.78E-04

The high loss tangent (tanδ) for the x = 0.0 sample is due to the huge resistance (2780663 Ω) of the grain boundary (R_{ins}) which is presented in Figure 4. It also seems that a significant reduction of tanδ in magnitude cannot be explained by a decrease in capacitance. Therefore, it is concluded that the notable reduction of tanδ by Y-substitution is occurred chiefly due to the attenuation of the resistivity of $La_{1-x}Y_xCoO_3$ (x = 0.0, 0.2, 0.4 and 0.6) grain/subgrains. In the case of Y^{3+} substitution for La^{3+}, Y acts as a donor. The doping of the donor usually increases the concentration of electrons in perovskite-type crystals and leads to the decrease the grain resistance. A close examination of the high-frequency regions indicates that the resistivity of the bulk (or grain) was changed negligibly by the Y doping. On the other hand, the resistivity contributed by the grain boundary decreased upon doping of Y. The impedance spectroscopy analysis indicates that

the conductivity of the semiconducting regions responsible for grains increases substantially with doping technique while the internal boundary layer (grain boundary) remains highly resistive, causing the notable decrease in the tanδ. In Table-5, generally, the α parameter expresses the deviation from the ideal Debye Equation and increases with increasing concentration of Y. R_{ins} decreases drastically with increasing Y concentration whereas R_{SC} decreases slowly.

Conclusion

In conclusion, polycrystalline $La_{1-x}Y_xCoO_3$ (x=0.0, 0.2, 0.4 and 0.6) were synthesized using standard solid state reaction process. The effects of the partial adding of Y^+ with La^+ on the structural, dielectric, and electrical characteristics of the samples in the frequency range of 20 Hz to 5 kHz at room temperature were understood from the X-ray diffraction and complex impedance spectroscopy analyses. The parents $LaCoO_3$ have a single phase rhombohedral perovskite type structure with space group $R\bar{3}c$, according to the x-ray diffraction study of $La_{1-x}Y_xCoO_3$. The Polycrystalline $La_{1-x}Y_xCoO_3$ exhibits a deformed perovskite type structure with a orthorhombic space group Pnma structure upon the addition of Y concentration. The electrical and dielectric characteristics of every sample have been studied. It was found that Y doping boosts conductivity, decreases dielectric loss, and increases capacitance. The contributions of the grain and grain boundary effects to the conductivity and dielectric loss of the examined samples were validated by Cole-Cole plots.

References

1. Chen Y., Qin H., Shi C., Li L. and Hu J., High temperature CO_2 sensing properties and mechanism of nanocrystalline $LaCrO_3$ with rhombohedral structure: experiments and ab initio calculations, *RSC Adv*., 2015, 5, 54710-54716.
2. Nasri, S., Hafsia A. L. Ben, Tabellout M. and Megdiche M., Complex impedance, dielectric properties and electrical conduction mechanism of $La_{0.5}Ba_{0.5}FeO_{3-\delta}$ perovskite oxides, *RSC Adv*., 2016, 6, 76659-76665.
3. Das, I., Chanda S., Saha S., Dutta A., Banerjee S., Bandyopadhyay S. and Sinha T. P., Electronic structure and transport properties of antiferromagnetic double perovskite Y_2AlCrO_6, *RSC Adv*., 2016, 6, 80415-80423.
4. Mattinez R., Kumar A., Palai R., Scott J. F. and Katiyar R., Impedance spectroscopy analysis of Ba0.7Sr03TiO3/La0.7Sr0.3MnO3 heterostructure, *J. Phys. D: Appl. Phys.,* 2011, 44, 105302-105310.
5. Shin Y. C., Hashimoto S., Yashiro K., Amezawa K. and Kawada T., Thermal Properties of Perovskite-Type Oxides $La_{0.6}Sr_{0.4}Co_{1-x}Fe_xO_{3-\delta}$ ($0 \le x \le 1.0$), *ECS Trans*., 2016, 72(7), 105-110.
6. Geffroy P.M., Vedraine S., Bouchiat F. D., Saha S. K., Gheno A., Rossignol F., Marchet P., Antony R., Boucle J. and Ratier B., Electrical and Optical Properties of $La_{1-x}A_xFe_{1-y}B_yO_{3-\delta}$ Perovskite Films (with A = Sr and Ca, and B= Co, Ga, Ti): Toward Interlayers for Optoelectronic Applications *J. Phys. Chem. C*, 2016, 120(50), 28583-28590.
7. Orlovskaya N., Kleveland K., Grande T. and Einarsrud M. A., Mechanical properties of $LaCoO_3$ based ceramics, *J. Eur. Ceram. Soc*., 2000, 20, 51-56.
8. Sakhya A. P., Rai D. P., Dutta S. A., Thapa R. K., and Sinha T. P., Electronic, optical and thermoelectric properties of PrMO3 (M=Al, Ga, In) from first-principles calculations†, *RSC Adv*., 2016, 6, 59988-59997.
9. Lee N., Lansac Y., Hwang H. and Jang Y. H., Switching mechanism of $Al/La_{1-x}Sr_xMnO_3$ resistance random access memory. I. Oxygen vacancy formation in perovskites, *RSC Adv*., 2015, 5, 102772-102779.
10. Ishihara T., Kudo T., Matsuda H. and Takita Y., Doped $PrMnO_3$ Perovskite Oxide as a New Cathode of Solid Oxide Fuel Cells for Low Temperature Operation, *J. Electrochem. Soc.*, 1995, 142(5), 1519-1524.
11. Ravichandran J., Siemons W., Heijmerik H., Huijbenx M., Majumdar A. and Ramesh R., An Epitaxial Transparent Conducting Perovskite Oxide: Double-Doped $SrTiO_3$, *Chem. Mater*., 2010, 22, 3983-3987.
12. Erdenee N., Enkhnaram U., Galsan S. and pagvajav A., Lanthanum-Based Perovskite-Type Oxides $La_{1-x}Ce_xBO_3$ (B = Mn and Co) as Catalysts: Synthesis and Characterization *J. Nanomater*., 2017, 2017, 9120586, DOI: 10.1155/2017/9120586.

13. Kato Y., Kaneko Y., Tanaka H., Baibara K., Koyama S., Isogai K., Yamaga T. and Shimada Y., Overview and Future Challenge of Ferroelectric Random Access Memory Technologies, *Jpn. J. Appl. Phys.*, 2007, 46, 2157

14. Chu P. Y., Jones R. E., Zurcher P., Taylor D. J., Jiang B., Gillespie S. J., Lii Y. T., Kottke M., Fejes P. and Chen W., Characteristics of spin-on ferroelectric $SrBi_2Ta_2O_9$ thin film capacitors for ferroelectric random access memory applications, *J. Mater. Res*., 1996, 11(5), 1065-1068.

15. Maurya D., Ahn C. W., Zhang S. and Priya S., High Dielectric Composition in the System Sn-Modified $(1-x)BaTiO_{3-x}$ $Ba(Cu_{1/3}Nb_{2/3})O_3$, x=0.025 for Multilayer Ceramic Capacitors, *J. Am. Ceram. Soc.*, 2010, 93(5), 1225-1228

16. Zhang Z., Chen Y., Tade M. O., Hao Y., Liu S. and Shao Z., Tin-doped perovskite mixed conducting membrane for efficient air separation, *J. Mater. Chem. A*, 2014, 2, 9666-9674.

17. Lvovich V. F., 2012, Impedance Spectroscopy, Applications to Electrochemical and Dielectrical Phenomena, John Wiley & Sons, New Jersey.

18. Bonanos N., Steele B. C. H. and Butler E. P., 2005, Impedance Spectroscopy Theory, Experiment, and Applications, John Wiley & Sons, New Jersey.

19. Sati P. C., Kumar M. and Chhoker S., Low temperature ferromagnetic ordering and dielectric properties of $Bi_{1-x}Dy_xFeO_3$ ceramics, *Ceram. Int.*, 2015, 41, 3227-3236.

20. Gogoi P., Srinivas P., Sharma P. and Pamu D., Optical, Dielectric Characterization and Impedance Spectroscopy of Ni-Substituted $MgTiO_3$ Thin Films, *J. Electron. Mater*., 2016, 45, 899.

21. Chao Z., Liu X., He W., Ruan X., Gao Y. and Liu J., Extrinsic and intrinsic contributions for dielectric behavior of La_2NiMnO_6 ceramic, *Phys. B*, 2015, 477, 8-13.

22. Coondoo I., Panwar N., Tomar A., jha A. K. and Agarwal S. K., Impedance spectroscopy and conductivity studies in $SrBi_2(Ta_{1-x}W_x)_2O_9$ ferroelectric ceramics, *Phys. B*, 2012, 407, 4712-4720.

23. Lefla R., Nasr F. B., Hrichi H. and Guermazi H., Optical, electrical properties and characterization of $(C_2H_5NH_3)_2CdCl_4$ compound, *Optik*, 2016, 127, 5534-5541.

24. Saghrouni H., Jomni S., Balgacem W., Hamdaoui N. and Beji L., Physical and electrical characteristics of metal/Dy_2O_3/p-GaAs structure, *Phys. B*, 2014, 444, 58-64.

25. Karatas S. and Kara Z., Temperature dependent electrical and dielectric properties of Sn/*p*-Si metal–semiconductor (MS) structures, *Microelectron. Reliab.*, 2011, 51, 2205-2209.

26. Fouad S. S., Sakr G. B., Yahia I. S., Abdel-Basset D. M. and Yakuphanoglu F., Impedance spectroscopy of p-$ZnGa_2Te_4$/n-Si nano-HJD, *Phys. B*, 2013, 415, 82.

27. Huang K., Lee H. Y. and Goodenough J. B., Sr- and Ni-Doped $LaCoO_3$ and $LaFeO_3$ Perovskites: New Cathode Materials for Solid-Oxide Fuel Cells, *J. Electrochem. Soc.* 1998, 145(9); 3220-3227.

28. Sinclair D. C., Adams T.B., Morrison, F.D., West A.R., $CaCu_3Ti_4O_{12}$: One-Step Internal Barrier Layer Capacitor, *Appl. Phys. Lett.,* 2002, **80,** 2153

29. Adams T.B., Sinclair D. C., Influence of Processing Conditions on the Electrical Properties of $CaCu_3Ti_4O_{12}$ Ceramics, *J. Am. Ceram. Soc.,* 2006, **89**, 3129.